The JWST MIRI Double-Prism, Design and Science Drivers

Sebastian Fischer[a] and Damian Moratschke[a] and Christian Straubmeier[a] and Andreas Eckart[a] and Laurence Rossi[b] and Jean-Yves Plesseria and Etienne Renotte and Emmanuel Mazy[b] and Jérôme Amiaux[c]

[a]1st Institute of Physics, University of Cologne, Zuelpicher Str. 77, 50937 Cologne, Germany;
[b]Centre Spatial de Liège, Avenue du Pre Aily, B-4031 Angleur-Liège, Belgium;
[c]Commissariat á l'Energie Atomique/DAPNIA, Orme des Merisiers, 91191 Gif-sur Yvette, France

ABSTRACT

We present how it is achieved to mount a double prism in the filter wheel of MIRIM - the imager of JWST's Mid Infrared Instrument. In order to cope with the extreme conditions of the prisms' surroundings, the low resolution double prism assembly (LRSDPA) design makes high demands on manufacturing accuracy. The design and the manufacturing of the mechanical parts are presented here, while 'Manufacturing and verification of ZnS and Ge prisms for the JWST MIRI imager' are described in a second paper [1]. We also give insights on the astronomical possibilities of a sensitive MIR spectrometer. Low resolution prism spectroscopy in the wavelength range from 5-10 microns will allow to spectroscopically determine redshifts of objects close to/at the re-ionization phase of the universe.

Keywords: JWST, MIRI, double prism, mount

1. INTRODUCTION

The purpose of the Low Resolution Double Prism Assembly (LRSDPA) is to allow for an integration of two prisms, made of Zinc-Sulfide and Germanium, accurately in the filterwheel of the MIRI imager. The low resolution spectroscopy mode of the MIRI imager then will allow to perform prism slit-spectroscopy in the wavelength-range from 5-10 microns at a resolution of R=100. This mode is particularly aiming at spectroscopic analyses of very low surface brightness objects, such as deeply embedded (proto-)stars, or the first light-emitting galaxies that re-ionized the universe shortly after the big bang.

A general problem in satellites is the limitedness of available room. The other main challenge is that the prisms, intrinsic fragile crystals, will be exposed to extremely high levels of vibrations during the launch of the rocket. The double prism assembly compensates for this and provides a safe mount of the prisms, with as few induced stress as possible. Springs provide a secure fixation - without overload - of the prisms, while gold-foils provide a soft contact between crystal and Aluminum parts. The mechanical design is developed by the University of Cologne (UoC), in collaboration with the Centre Spatial de Liège (CSL). Manufacturing of the two prisms is provided by AMOS [1], all other high-precision manufacturing is performed by the fine mechanical workshop of UoC's 1st Institute of Physics.

Starting with a scientific motivation on why the low resolution spectroscopy mode is essential for the science aims of JWST, the following chapters will explain in more detail how the prisms are mounted, and what critical aspects had to be considered in the design. The test campaigns in order to qualify the performance of the LRSDPA are described in [1].

Contact details: fischer@ph1.uni-koeln.de, phone ++49 +221 470 3552, fax ++49 +221 470 3562; http://www.astro.ph1.uni-koeln.de

Space Telescopes and Instrumentation 2008: Optical, Infrared, and Millimeter,
edited by Jacobus M. Oschmann, Jr., Mattheus W. M. de Graauw, Howard A. MacEwen,
Proc. of SPIE Vol. 7010, 70103K, (2008) · 0277-786X/08/$18 · doi: 10.1117/12.788672

2. SCIENCE DRIVERS

For an extensive discussion of the scientific fields of JWST, we refer to [2]. The natural field of appliance for a sensitive MIR spectrometer is to spectroscopically study higher-redshifted counterparts of the galaxies in our local universe. For example, at a redshift of z = 3, the Near-infrared J, H and K-bands ($\lambda = 1.252.4\,\mu$m) are shifted into the 5 - 10 μm band of the LRS mode. These observations yield information on the evolution of galaxies and AGN over cosmic timescales. Hence local spectroscopic infrared studies [e.g. 3] can be expanded to larger lookbacktimes with a reasonable amount of integration time compared to ground-based MIR telescopes, which suffer from the high thermal background.

However, one of the most ambitious scientific aims of the James Webb Space Telescope is the detection of the first bright objects in the universe - which ended the cosmic 'Dark Ages': At about 180 million years after the Big Bang, [4], the initially hot universe expanded and cooled down below the sublimation temperature of hydrogen molecules. This allowed for the formation of the very first stars in the universe, which consisted only of hydrogen and helium. Due to the lack of sufficient cooling mechanisms in these zero metallicity stars, their effective temperature is of the order of $10^5\,K$ [e.g. 5]. On the one hand, this causes the Jeans mass to be much higher than for solar mass metallicities. Hence, zero metallicity stars favor masses of $> 100\,M_\odot$. On the other hand, this means that these sources are very effective in ionizing hydrogen and helium. However, the high effective temperatures imply also low UV / optical fluxes: The spectral energy distribution of these stars at temperatures of $\sim 10^5\,K$ follows that of a black body of corresponding T_{eff}. Here, UV and optical band fall into the Rayleigh-Jeans limit, where the flux of the bolometric luminosity function scales with T_{eff}^{-3}. Most recent results from the Hubble Ultra-Deep Field observations predict that this process of re-ionization was ignited at redshifts of $z_{reion} = 15 \pm 5$ [6]; WMAP observations of the cosmic microwave background result in a redshift of $z_{reion} = 10.9^{+2.7}_{-2.3}$ [7]. At these redshifts, the restframe UV / optical gets shifted into the mid-infrared. Still, the faintness of these stars makes observations challenging, even for JWST. [8] discuss that JWST will not be able to determine metallicities for low-metallicity starburst objects at a spectroscopic resolution of R=1000. Here MIRI's double prism low resolution spectroscopy mode (R=100) becomes crucial due to its increase in sensitivity. For the brightest zero-metallicity star clusters and dwarf galaxies, the LRS mode is able to not only determine redshifts, but also to give estimates on their metallicity. For example, as can be seen in Fig. 1, the [OIII]- and HeII lines are sensitive indicators to changes in metallicities and at the expected redshifts readily accessible for the LRS mode.

3. DESIGN DRIVERS

The base of the LRSDPA is the optical layout, and the respective requirement specifications, developed by the Commissariat á l'Energie Atomique (CEA), the lead MIRI imager team. The positioning accuracy of the prisms inside the holder, the enormous levels of accelerations and the tight allocated outer envelope all have serious impacts on the final design.

The design presented in this paper is a redesign of the LRSDPA's demonstration model structure which was presented in [9]. Initially designed for much lower loads (i.e. 20 gRMS), one of the two prisms was not able to withstand the final applicable axial random vibrations during the DM vibration test campaign. The redesign has issued this problem and optimized the prisms' robustness. Its success has already been proven by the successful qualification of the vibrational test campaign.

3.1 Design Overview

The great two advantages of the low resolution spectroscopy double prism assembly which motivated its implementation into JWST are that it

1. yields a very effective light-throughput and allows spectroscopy of *very* faint targets (efficiency of $\sim 80\,\%$;
2. provides light dispersion without altering the beam angle, similar to a photometric filter. This means it can be implemented into an imager without the need for additional optics.

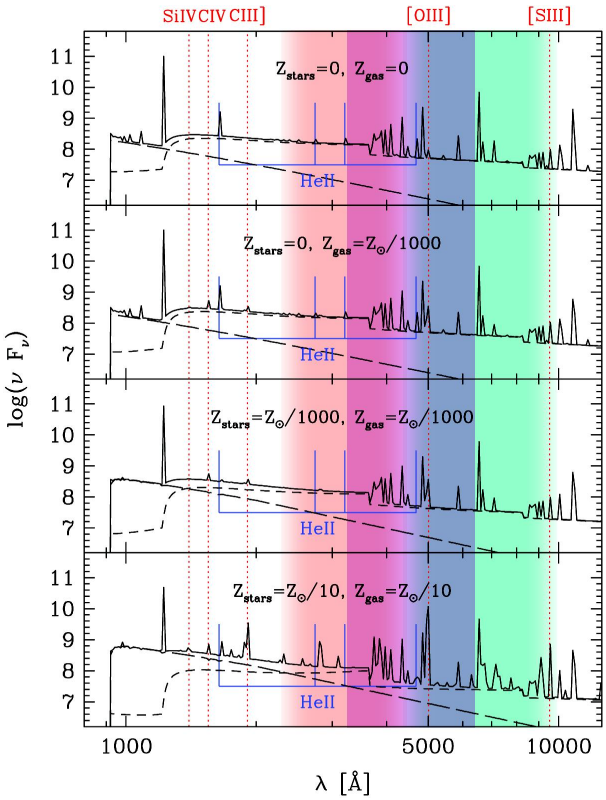

Figure 1. Taken from [8]: The synthetic spectrum of a zero-metallicity HII region (top panel) is compared to that of HII regions with various combinations of stellar and nebular metallicities (lower panels). The long-dashed and short-dashed lines represent the stellar and nebular continua, respectively. In addition, the 5-10 μm band corresponding to a redshift of $15^{+5\,(red)}_{-5\,(blue)}$ is overlayed.

The use of a grism, although more compact, would lead to an unrealistic number of grooves per mm to achieve the desired resolution (4 grooves per mm would be required). The optical layout of the low resolution spectroscopy mode is presented in Fig. 2. The first of the two prisms is made of Germanium (Standard Grade), the second prism's material is Zinc Sulfide (MultiSpectral Grade). Characteristic for both prisms is an extremely high refraction index in the mid infrared (, at $\sim$ 50 K and 7.5 μm: $n_{Ge} = 3.92$, $n_{ZnS} = 2.22$, [10]).* The diameter of the prisms are 23.4 mm (Ge) and 24.5 mm (ZnS). To reduce the amount of stray-light in the spectrum, the two optical surfaces of each prism are coated with an anti-reflective coating optimized for the wavelength range from 5 μm - 10 μm. In addition, the optical design foresees diaphragms in the shape of the JWST footprint on the front and exit faces of the prism. From stray-light concerns, one of these diaphragms is completely sufficient, and in the LRSDPA this diaphragm is incorporated into the cover of the Ge prism. For sensitivity as well as stray-light reasons, the surfaces of all mechanical parts are black anodized.

The pixel scale of the resulting spectrum is roughly 28 pixels / μm. According to the Rayleigh criterion, the spectrum will show a resolution of 100 at 7.5 μm. This implies that the spectrum will be Nyquist sampled. The operating temperature of the double prism is, like the operating temperature of the whole MIRI imager, 7 K. The sensitivity of the spectrometer aims at $0.6\,10^{-20}\,W/m^2$ *for line flux and* 1.35 μJy *on the continuum flux (10σ detection after 10000s).*

3.1.1 Structural Concept

The goal of the structural design is to induce as few stress as possible into the optically active volume of the prisms, while providing an accurate alignment. Therefore, a semi-kinematic mounting of the prisms via an

*However, a disadvantage of especially the ZnS crystal is a large spread of refractive inhomogeneity which claims much of the tolerance budget distribution of the requirements specifications.

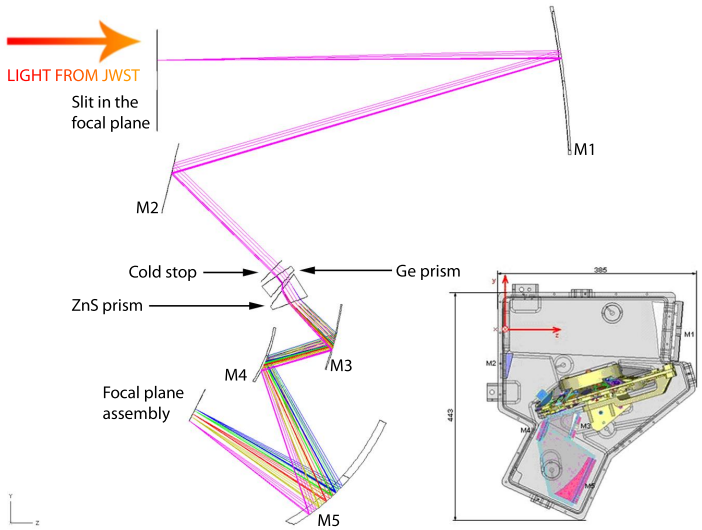

Figure 2. Optical Layout of the LRSDPA. The mid infrared light enters the imager from a pick of mirror through the LRS slit. After several reflections and focusing, the light enters the double prism assembly (entrance Ge prism, exit ZnS prism), is dispersed, and after 3 more reflections is focused onto the detector. Note that the double prism light dispersion does not alter the angle of the beam, what allows for an implementation into an imaging unit. On the bottom right, the imager CAD model with its filterwheel is shown in the same orientation.

interface-flange attached to the prisms is chosen. In particular, the design accomplishes that *under all appearing accelerations, the LRSDPA behaves completely rigid, i.e. no displacement of a prism (which would inevitably lead to its destruction) occurs.*

Fig. 3 shows an exploded view of the LRSDPA. All individual components of the LRSDPA are shown in the order of their implementation. The structural concept is summarized as follows (any tolerancing is explained in detail in section 3.3):

- The main mounting structure houses the two prisms and provides the interface to the filterwheel. The LRSDPA is attached to the filterwheel via 3 M3 hexalobular socket head screws (steel AISI 316 A4). The alignment with respect to the filterwheel is secured by two dowel pins.
- Most components of the LRSDPA (with the exception of the prisms themselves, the screws, the springs and two gold-foils located on the prisms flanges) are made of Al 6061 T6. The Aluminum parts have been thermally tempered to improve the structural hardness prior to fine machining (cooled down to 77 K for >20 h, then cycled several times between 423 K and 290 K).
- The prisms' optical alignment is provided by the fit of the prism into the holder. No further manual adjustments / alignment are required.
- The two prisms each have a large flange attached to the optically active volume. The interface to the holder is completely realized using only this flange. Especially, the entrance and exit faces of the prisms are free from any contact.
- In order to avoid the generating of microcracks, which could propagate through the crystal during vibrations or thermal cycling, the surfaces of the prisms are lapped where this is feasible. This includes the flange and the main body of the prism (from a stray-light-point-of-view, this is not recommended; however, it is highly favorable to improve the prisms structural capabilities).
- A hard Aluminum-crystal contact is not desired. Gold foils with a thickness of 25 μm are placed on bottom and top of the prisms' interface flanges.

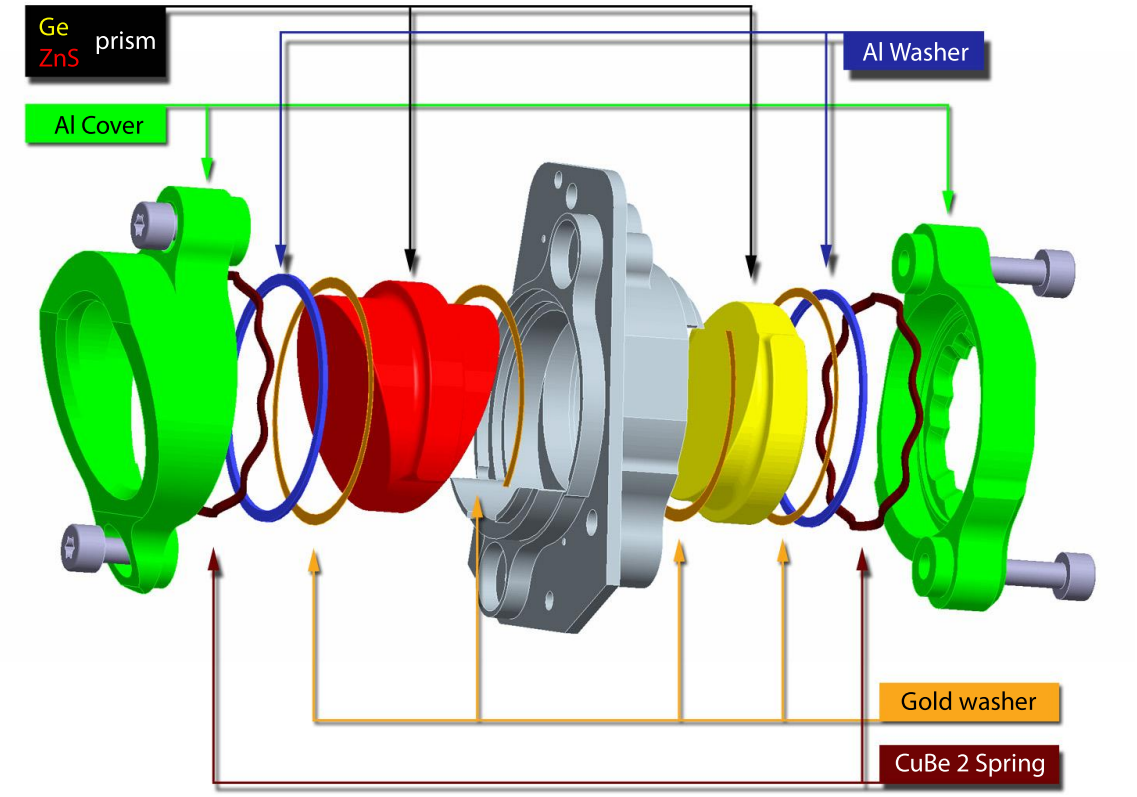

Figure 3. An exploded view of the LRSDPA and its components.

- The semi-kinematic mounting is realized with one CuBe 2 ondulated spring per prism. The springs contract to a height of 1.5mm under their respective preload. The overall contraction is only $0.100\,\mathrm{mm} \pm 0.05\,\mathrm{mm}$.
- The spring compensates a quasistatic force of $3 * 55\,\mathrm{g}$ in axial direction directly. $3 * 33.1\,\mathrm{g}$ quasistatic forces in lateral directions are compensated via static friction. Since the prisms differ in size and mass, different springs for the Ge prism and the ZnS prism are needed.
- According to simulations, both prisms will survive the expected accelerations with a positive margin of safety > 2.4 (3.4 for the Ge prism, 3.8 for the ZnS prism, see section 3.2).
- Due to the small available space, the springs have only 6 waves. In order to avoid point-loads induced onto the prisms, an Al6061 T6 washer (0.5mm thickness) is placed between prism and spring.
- To minimize stray-light, diaphragms are needed at the outer surfaces of the prisms. A mask representing the beam (including pupil shear) is included in the cover of the Ge prism. On the exit surface of the ZnS prism, an elliptically shaped mask, surrounding the telescope footprint, is sufficient for the avoidance of stray-light and allows for an technically easier manufacturing.

The mass of the LRSDPA is 75.9 g. Based upon calculations, the center of gravity is located at

$$(-0.17444, -151.02637, 91.85781)\,\mathrm{mm}$$

with respect to the global MIRI imager coordinate system (see Fig. 2) and the principal moments of inertia are

$$(8.5307, 12.2903, 12.87266)\,\mathrm{kg/mm^2}.$$

Due to the compactness of the LRSDPA, its Eigenfrequencies are high. Simulations resulted in a first Eigenfrequency of the LRSDPA at a frequency of 6.04 kHz (Table 2). This is conform with the qualification tests, where

Table 1. Material properties of the materials in use for the LRSDPA. Contraction refers to a thermal contraction between 293 and 4 K. Values taken from LAKESHORE, GOODFELLOW, and MATWEB

Material	Density [g / cm^3]	Contraction (10^{-4})	Poisson Ratio	Young's Modulus [10^{10} Pa]
Al6061 T6	2.71	41.4	0.3	6.89
Steel AISI 316 A4	7.8	30	0.29	21.50
CuBe 2	8.25	49.3	0.3	12-16
Ge std-grade	5.323	9.3	0.28	10.27
ZnS MS-grade	4.09	9.5	0.29	7.45

Material	Ultimate Tensile Strength [N /mm^2]	Specific Heat [J / g / K]	T. Conductivity [W / m / K]
Al6061 T6	430	0.964	180.07
Steel AISI 316 A4	580	0.500	16.3
CuBe 2	NN	0.419	90-130
Ge std-grade	95±48	0.310	58.61
ZnS MS-grade	69	0.515	27.2

Table 2. Modal Modes and Mass Participation Factors of the LRSDPA. Z is the vertical axis (along the prism generating axis, X and Y the lateral axes. From the mass participating factors, one can see that the 1st Eigenmode is an oscillation along the axial direction, whereas the 2nd and 3rd Eigenmodes are almost completely oscillating in the lateral direction.

Eigen-mode	Frequency [kHz]	Participating mass factors X [%]	Y [%]	Z [%]
1	6.403	13.6	4.8	1.7
2	6.582	0.0	17.7	28.6
3	8.110	0.1	28.5	1.8

in a frequency-sweep from 20-2500 Hz, no Eigenfrequency has been found. For these calculations, it has been assumed that the LRSDPA behaves as one rigid part, where no movement of any sub-part is allowed. As long as the excitation loads do not exceed the design loads, this assumption is reasonable.

3.2 Geometric Elements Method Analyses

During the design phase, the characteristic response of the two prisms to the expected maximum acceleration levels were studied using the software *Pro/Mechanica*. The simulation technique applied by Pro/Mechanica is a geometric elements method simulation (GEM simulation). This means that convergence of the simulation is acquired by increasing the polynomial order of the mesh which represents the structural part (in contrast to finite model simulations, where convergence is achieved by decreasing the size and increasing the number of elements). Simulations of the complete LRSDPA in assembly-mode were too time-consuming and did not converge. Hence, the prisms are investigated individually.

Ultimate ambition of the design of the two prisms is that simulations verify the prisms' ability to withstand appearing accelerations and induced stresses by a safety factor of 2.4 concerning the ultimate stress limit(Astrium / ESA agreement).[†] The actual prisms are mounted using a spring which presses onto the prism's flange. For the GEM-study, this semi-kinematic mount has been idealized:

- The prism is constrained versus displacement in x- direction[‡] via the underside of the prism's interface flange and in y- and z-direction via the vertical edge of the same flange.

[†]For optical materials, there is no general ECSS safety factor defined, here case-by-case margins have to be agreed upon. For comparison, ECSS-E-30 suggests a safety-factor of 1.5 concerning ultimate stress limits for any metallic materials used in mechanisms.

[‡]For each prism, a dedicated coordinate system was used for the simulation. The x-axis of this coordinate system coincides with the generating axis of the prism's cylinder and the z-axis lies in the symmetry-plane of the prism.

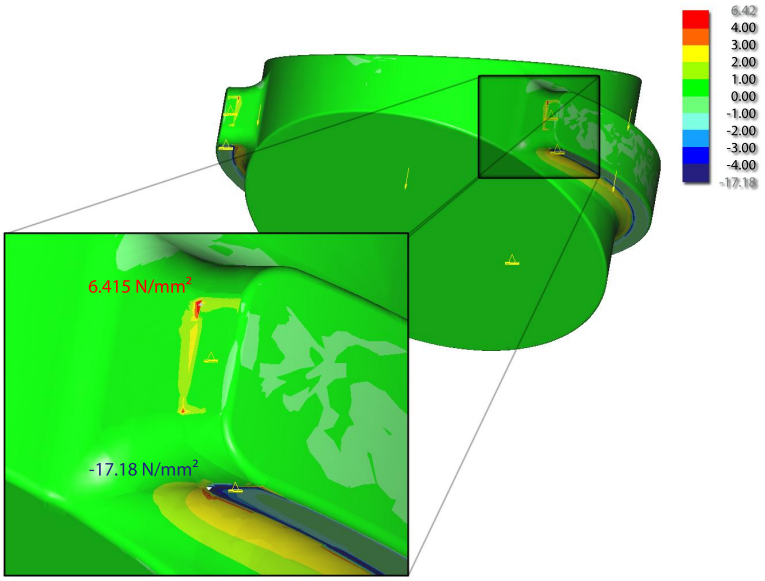

Figure 4. The Maximum Principal Stresses are shown color coded in units of MPa. Highest levels of stress are located at the prism's flange, whereas the main body of the prism is kept free of stress. With respect to an ultimate tensile strength for ZnS of 68.9 MPa, the prism will survive the applied loads within a safety factor of 3.8.

- The required preload, which in reality is provided by the CuBe 2 spring, is applied axially onto the flange. According to the definition of the random vibration design levels, 55 gRMS in axial and 33.1 gRMS in radial direction must be expected. For the calculation of the preload of the spring, the following aspects are considered:
  - The radial fixation of the prism is accomplished via static friction. A coefficient of static friction of $\mu = 0.25$ is used to represent the prism-goldfoil-Aluminum contact.[§]
  - A safety margin of an increased load of 10% is multiplied to the random levels.
  - Due to manufacturing and tolerancing budget, only 85% of the preload are effectively mounting the prism.
- In addition, 166 g (= 55.13 gRMS $*$ 3) gravity are considered in axial direction.

In this way, preload and gravity are acting in the same direction, inducing the largest amounts of stress into the prisms (i.e. worst case study). For both prisms, convergence of the simulation was reached within 10% in the criteria of edge displacement, element strain energy, and global RMS stress. This is sufficient for a rough estimate of the prisms survivability during random vibrations. The maximum polynomial order for the simulations is 9.

The ultimate tensile strength of ZnS multi spectral grade is **68.9 MPa**. The result in Fig. 4 shows that the highest stress-values occur at the edge of the flanges surfaces which provide contact to the holder, near its front-edge. However, the maximum principle stresses do not exceed 18 MPa (maximum model value is 6.4 MPa, minimum model value is -17.2 MPa). According to this, the ZnS prism will survive the applied loads within a safety factor of 3.8 (a safety factor of the demanded 2.4 results in an effective stress limit of 28.7 MPa).

The ultimate tensile strength of Ge standard grade is (95 ± 16) MPa ($1\,\sigma$ error). To be conservative within a $3\,\sigma$ error, we consider an **ultimate tensile strength of 47 MPa**. With a SF of 2.4, we aim at a stress limit for our study of 19.6 MPa. In Fig. 7, the maximum principal stresses are shown. The stresses are distributed similar to the distribution in the ZnS prism, at the inner edge of the constrained contact areas (near the front face of the flange). The simulation geometry is somewhat idealized due to a rounding at the edge of the flange

[§]Since 33.1 gRMS / 0.25 $>$ 55 gRMS, the **radial** random vibration levels are driving the preload of the spring!

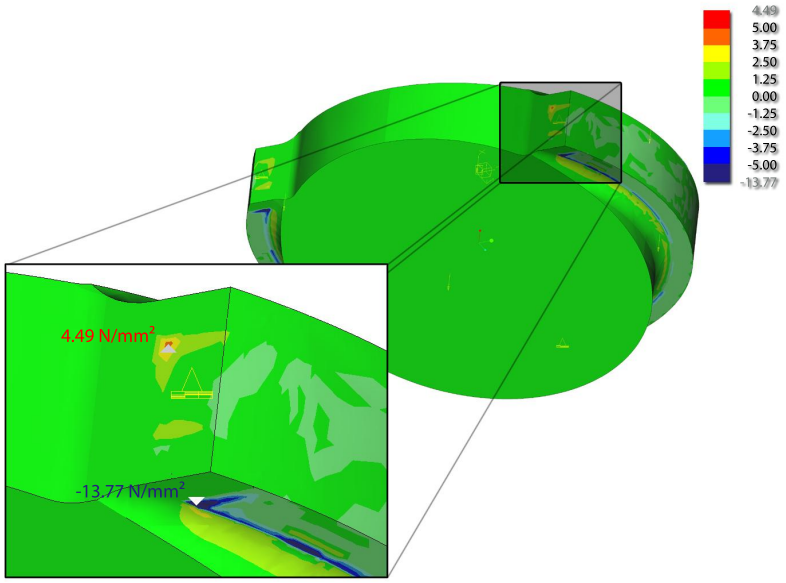

Figure 5. The Maximum Principal Stresses are shown color coded in units of MPa. Similar to the ZnS prism analysis, highest concentrations of stress are located at the prism's flange, while the main body of the prism is kept free of stress. With respect to a $3\,\sigma$ ultimate tensile strength for Ge of 47 MPa, the prism will survive the applied loads within a safety factor of 3.4.

causing a singularity during initial runs. Hence, the real-life situation with rounded edges should have an even better stress distribution than the simulation shown here. The maximum principal stresses do not exceed a value of 14 MPa (model max. value is 4.5 MPa, model min.value is -13.8 MPa), equal to a safety factor of 3.4 with respect to the $3\,\sigma$ ultimate tensile strength limit.

3.3 Tolerancing

The requirements of positioning of the prisms are met just by integrating the prism into the holder, no further alignment of the prism is needed / possible. The positioning requirements are defined for cold conditions (8 K) of the LRSDPA. Since no metrology of the alignment of the prisms in an assembled LRSDPA at can be achieved at cold conditions, it is important to prove that the strategy of radial alignment by design is in accordance with these requirements. The distribution of the tolerance budget between the different components has been achieved in close communication with AMOS, the supplier of the prisms, and the workshop of the 1st Institute of Physics. For most dimensions, the philosophy was to allow the manufacturing of the prism crystals to constrain the distribution of the tolerance budget, i.e. the larger budget is allocated to the prism manufacturing.

To meet the required *vertical* positioning accuracy of 0.07 mm, the holder provides a rigid contact to the prism (i.e. the prism's flange) with a respective bearing surface inside the holder. The holder's bearing surfaces are machined to a precision of $10\,\mu$m with respect to the dowel pin holes, which is the accuracy-limit that can be reached with our 5-axis CNC milling machine. The bearing surface of the prisms' interface flanges have a tolerance of 0.03mm with respect to its optical surface. Considering the flatness of the contact surfaces, 0.005 mm each, the prisms are placed in z-direction to an accuracy of ± 0.05 mm. In *lateral* direction, the prisms are positioned against displacement via their cylindrical shape. The machining tolerances are calculated such that the positioning at 8 K fulfills the required $\pm\,0.100\,mm$ with an additional restriction that a warm prism still fits into a cold holder[¶]. AMOS is able to machine the diameter of the prism up to an accuracy of $\phi\,^{+0.005}_{-0.020}$ mm, where the smaller upper limit again avoids the risk of a too small gap between holder and prism. The rotational movement around the axis of the prism (*roll*) is restricted by the front face of the prism's flange.

[¶]To avoid any risk of thermally induced stresses due to differential thermal expansion between the Aluminum holder and the prism materials.

Table 3. The required positioning accuracy is compared to the achieved accuracy by the design. These values are for cold conditions and hence cannot be verified through measurement. However, careful transfer of these requirements to ambient temperatures (see text for details) provides that metrology of the individual LRSDPA components (cf. chapter 4) can verify the compliance to the requirements. The positioning accuracy concerning roll α is a bit larger than the roll-accuracy concerning β, because the prism's flange is not fully closed.

		Achieved Accuracy	
Description	Requirement	Ge Prism	ZnS Prism
Δx, Δy	$\pm 100\,\mu$m	$\pm 100\,\mu$m	$\pm 100\,\mu$m
Δz	$\pm 70\,\mu$m	$\pm 50\,\mu$m	$\pm 50\,\mu$m
$\Delta \alpha$	$\pm 0.027^o$	$\pm 0.021^o$	$\pm 0.020^o$
$\Delta \beta$	$\pm 0.027^o$	$\pm 0.026^o$	$\pm 0.026^o$
$\Delta \gamma$	$\pm 0.250^o$	$\pm 0.19^o$	$\pm 0.12^o$

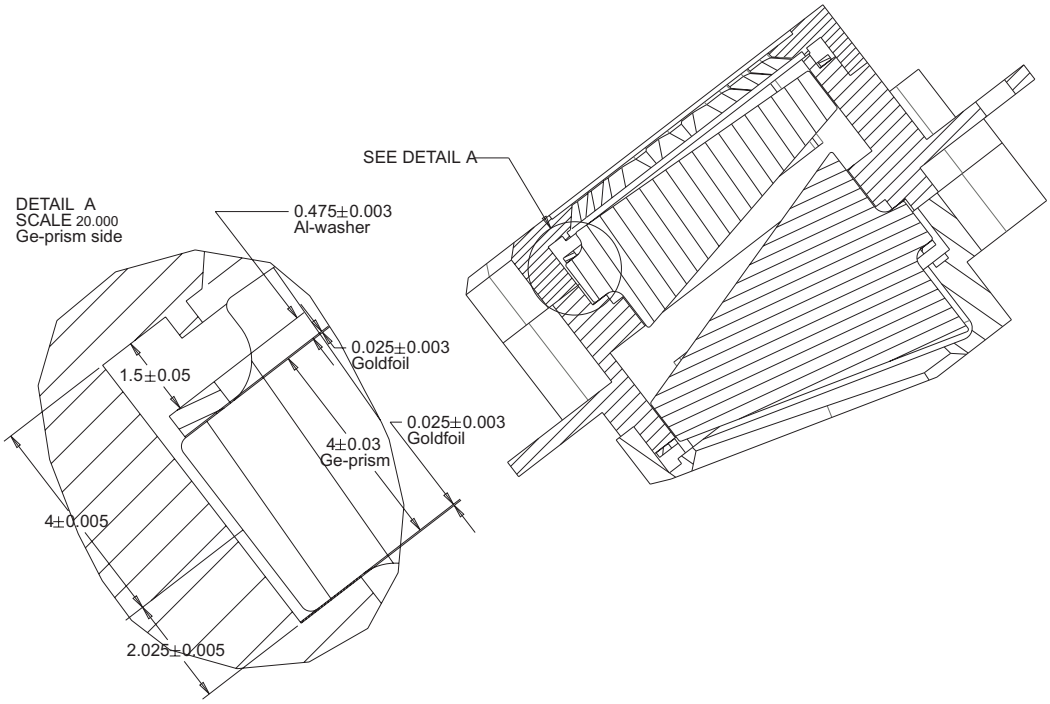

Figure 6. The overall tolerance budget distribution for the (significant) vertical dimensions of all participating components are shown, exemplary for the Ge-prism side of the holder (ZnS prism side is analogous). Goal is a contracted height of the spring of (1.50 ± 0.05) mm, which results in a compression of the spring of 0.1 mm ($\pm 50\%$). The budget adds up as indicated above.

Besides the demand for high accuracy positioning, there is another critical aspect concerning the manufacturing tolerances. Taking all tolerances into account, the spring which mounts the prism onto the holder has to be contracted sufficiently. Otherwise, its purpose of fixing the prism against movement during launch vibrations, is not guaranteed, and with the enormous expected accelerations, any movement of a prism can eventually lead to the prism's destruction.

4. LRSDPA QM, FM &FS PARTS

The two prisms of the LRSDPA are provided by AMOS, and their manufacturing is described in detail in [1].

All other parts for the LRSDPA qualification, flight and flight spare model are provided by University of

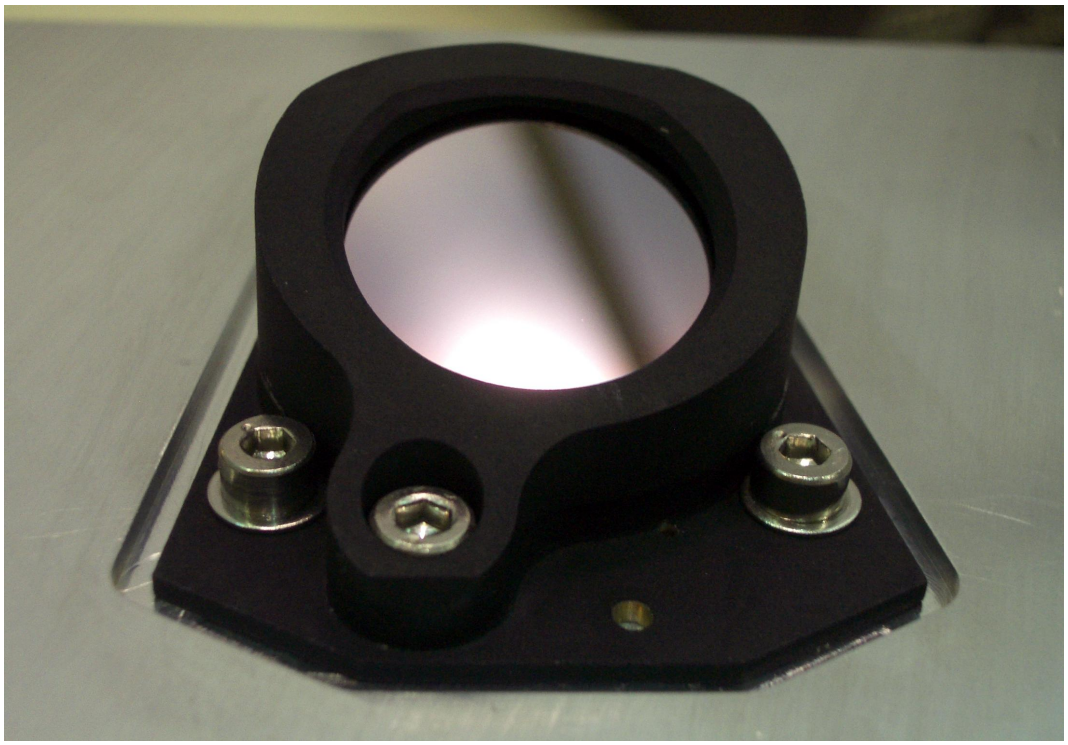

Figure 7. The flight model of the LRSDPA (view onto the ZnS side).

Cologne. Most components are milled on a 5-axis CNC milling machine. Concerning crucial dimensions, this machining is performed up to a precision of 5 μm. Due to the difficult shape of the holder and the two covers, standard metrology was not sufficient to obtain significant data. Hence, we relied on the 3D metrology of the Institut für Bildsame Formgebung at the University of Aachen, using an ATOS SO camera system. For a complete set of 6 holders and covers we obtained metrology and selected the 3 best sets for QM, FM and FS. Some exemplary metrology data is shown in Figure 8.

To verify the performance of the CuBe2 springs produced by UoC, the contraction of the spring under increasing load has been measured with micrometer precision. The final resulting curves are presented in Figure 9. Prior to the measurement of these curves, the springs have been exposed to more than 20 contractions to 1.500mm, a load of 39kg, and shock cooling with liquid nitrogen bath (for more than 1minute). All springs provide the required load under their 'maximum' contracted height.

5. OUTLOOK

The QM vibration qualification campaign has been successfully finished, as has the FM vibration campaign at acceptance levels. At the time of writing of this paper, the QM is currently being thermally cycled, with the FM cycling pending. The delivery date so far is on schedule with a delivery of the FM to CEA planned for mid of June. Then, the FM will be integrated into the MIRI imager's filterwheel for continuing qualification.

The launch of JWST is planned for 2013.

ACKNOWLEDGMENTS

This work is supported by the German federal department for education and research (BMBF) under the project numbers: 50OS0502 & 50OS0801.

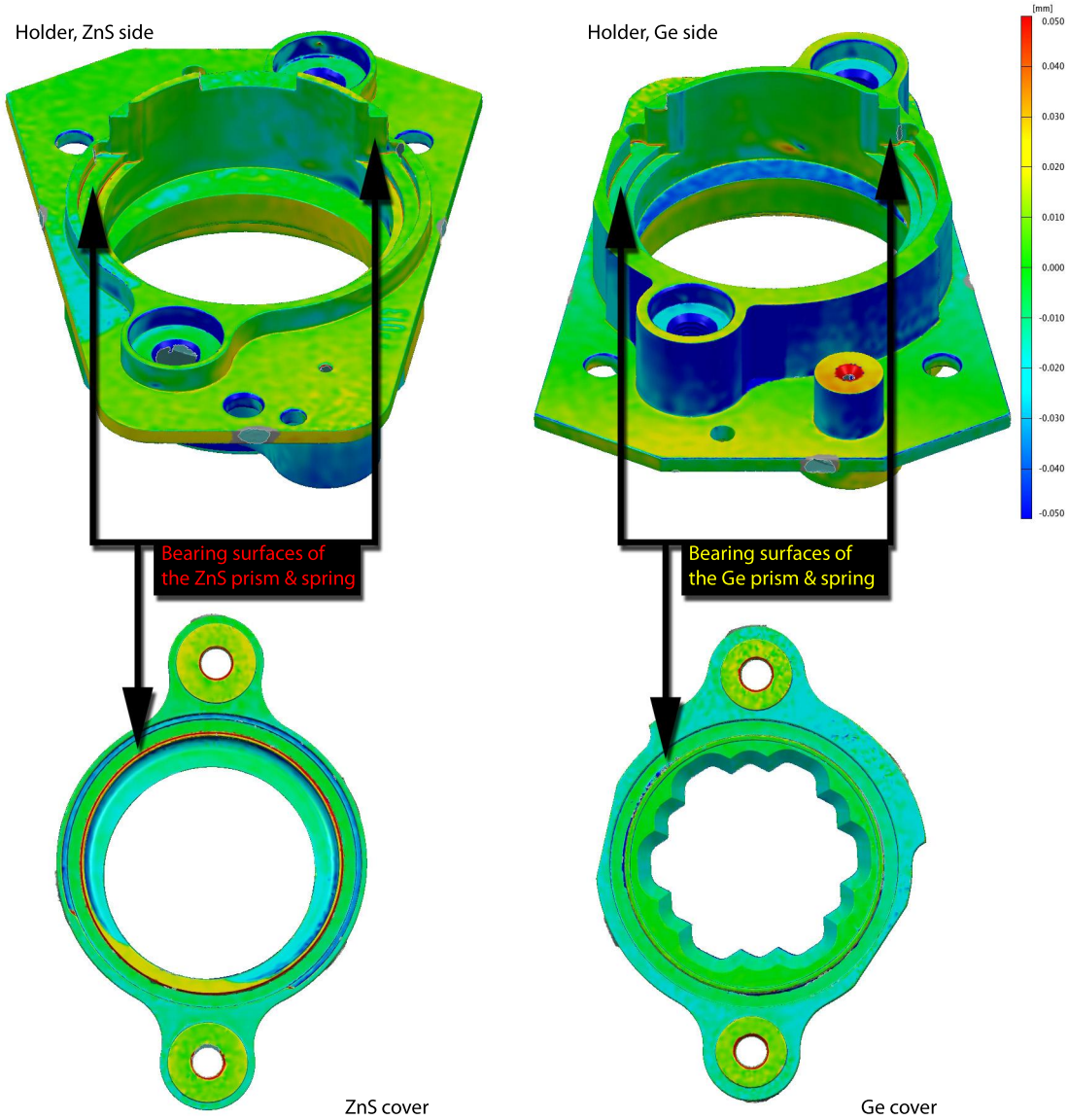

Figure 8. Exemplary 3D metrology results of holders and covers. The color-code refers to the comparison between reconstructed 3D model and the nominal design (red is positive deviation of 0.05mm, blue negative deviation of 0.05mm, green is 0.00mm deviation). The high conformity of the surfaces relevant for positioning of the prisms is obvious. The metrology has been achieved at the Institut für Bildsame Formgebung, University of Aachen.

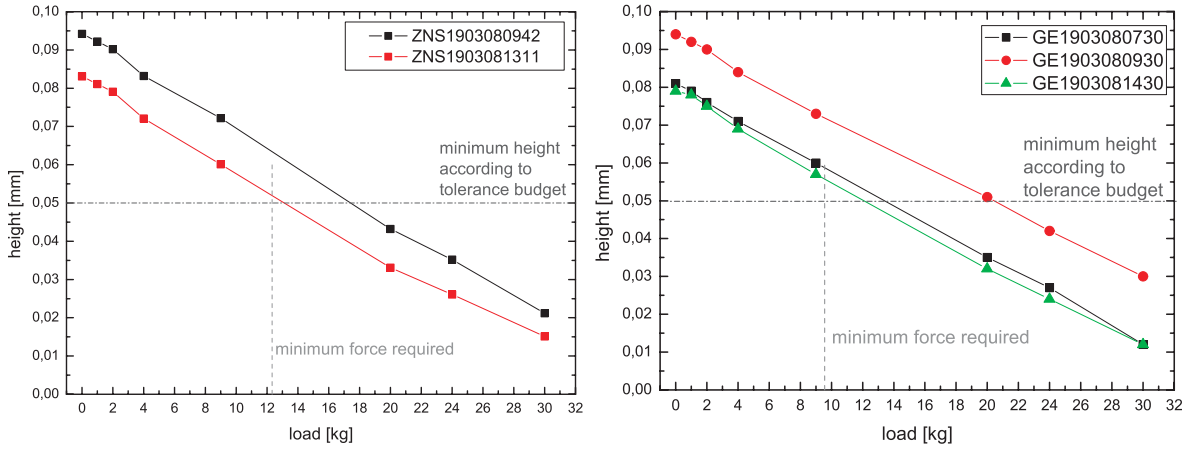

Figure 9. Characteristic diagrams of the FM and FS springs produced by UoC. In the diagrams, the minimum contraction (dash-dotted line) and the minimum required force (dashed line) are indicated; a height of 0.00mm corresponds to a spring contracted to 1.50mm. All springs fulfill the requirements. GE1903080730 and GE1903081430 will be used for FM and FS. The linearity of the force-contraction behavior is characteristic of only minor discrepancies to the ideal dimensions of the spring design.

REFERENCES

[1] Rossi, L., Ninane, N., Mazy, E., Plesseria, J.-Y. D., Renotte, E., Wielandts, M., Fischer, S., Straubmeier, C., Dubreuil, D., Amiaux, J., Poupar, S., and Ronayette, S., "Manufacturing and verication of zns and ge prisms for the jwst miri imager," *Space Instrumentation and Cryogenics I. Proceedings of the SPIE.* **7018**, 76 (2008).

[2] Gardner, J. P., Mather, J. C., Clampin, M., Doyon, R., Greenhouse, M. A., Hammel, H. B., Hutchings, J. B., Jakobsen, P., Lilly, S. J., Long, K. S., Lunine, J. I., McCaughrean, M. J., Mountain, M., Nella, J., Rieke, G. H., Rieke, M. J., Rix, H.-W., Smith, E. P., Sonneborn, G., Stiavelli, M., Stockman, H. S., Windhorst, R. A., and Wright, G. S., "The james webb space telescope," *Space Science Reviews* **123**, 485–606 (2006).

[3] Rodrguez-Ardila, A., Binette, L., Pastoriza, M. G., and Donzelli, C. J., "The narrow-line region of narrow-line seyfert 1 galaxies," *Astrophysical Journal* **538**, 581–593 (2000).

[4] Barkana, R. and Loeb, A., "In the beginning: the first sources of light and the reionization of the universe," *Physics Reports* **349**, 125–238 (2001).

[5] Bromm, V., Kudritzki, R. P., and Loeb, A., "Generic spectrum and ionization efficiency of a heavy initial mass function for the first stars," *Astrophysical Journal* **552**, 464–472 (2001).

[6] Panagia, N., Fall, S. M., Mobasher, B., Dickinson, M., Ferguson, H. C., Giavalisco, M., Stern, D., and Wiklind, T., "Direct evidence for an early reionization of the universe?," *Astrophysical Journal* **633**, L1–L4 (2005).

[7] Spergel, D. N., Bean, R., Dor, O., Nolta, M. R., Bennett, C. L., Dunkley, J., Hinshaw, G., Jarosik, N., Komatsu, E., Page, L., Peiris, H. V., Verde, L., Halpern, M., Hill, R. S., Kogut, A., Limon, M., Meyer, S. S., Odegard, N., Tucker, G. S., Weiland, J. L., Wollack, E., and Wright, E. L., "Three-year wilkinson microwave anisotropy probe (wmap) observations: Implications for cosmology," *Astrophysical Journal Supplement Series* **170**, 377–408 (2007).

[8] Panagia, N., "The quest for primordial stellar populations and the james webb space telescope," *Chinese Journal of Astronomy and Astrophysics Supplement* **3**, 115–125 (2003).

[9] Fischer, S., Straubmeier, C., Eckart, A., Rossi, L., and Mazy, E., "Mounting miri's double prism," *Space Telescopes and Instrumentation I: Optical, Infrared, and Millimeter. Edited by Mather, John C.; MacEwen, Howard A.; de Graauw, Mattheus W. M.. Proceedings of the SPIE, Volume 6265, pp. 62653A (2006).* **6265**, 101 (2006).

[10] Hawkins, G. J., "Spectral characterisation of infrared optical materials and filters," *The University of Reading, Department of Cybernetics.* **PhD-Thesis** (1999).